MECSOL Joinville 2017
April 26-28, 2017
Joinville, Santa Catarina, Brazil

Acoustic Emission tests: Simulations using Lattice Discrete Element Method

Gabriel Birck
Department of Mechanical Engineering
Federal University of Rio Grande do Sul, Porto Alegre, RS, Brazil
Univates University Center, Lajeado, RS, Brazil
gabriel.birck@ufrgs.br

Ignacio Iturrioz
Department of Mechanical Engineering
Federal University of Rio Grande do Sul, Porto Alegre, RS, Brazil
ignacio@mecanica.ufrgs.br

ABSTRACT

The methods proposed to predict the damage process in quasi-brittle materials may be classified into two large groups: those based on continuum mechanics, i.e. the so-called classical approach and the statistical models approach. In the first, plasticity theories are extended to study the damage process, leading to procedures that encounter serious difficulties when dealing with quasi-brittle materials, in which scale effects, anisotropic damage and associative defects are likely to occur. The statistical model approach consist on simulate the solid with a set of nodes where the solid mass is dumped are interlinked with interaction functions that as in whole represent the solid behaviour. The formulation presented in this work is a particular case of the second group, called Lattice Model, namely LDEM. This model is based on the representation of a solid by means of a cubic arrangement of elements able to carry only axial loads. This approach takes into account the irreversible effects of crack nucleation and propagation bars. In the present work, three applications are presented with the aim to illustrate how the simulation of Acoustic Emission tests let understand the behaviour of the damage process in quasi-brittle materials. The results obtained in the simulation are useful to understand the experimental ones. Therefore, LDEM can be auxiliary tool for the interpretation of Acoustic Emission tests.

Keywords: Heterogeneous materials, Lattice Model, Acoustic Emission Technique, Damage Process

1. INTRODUCTION

From a physical point of view, damage phenomena consist either of surface discontinuities in the form of cracks or of volume discontinuities in the form of cavities [1, 2]. Macroscopically, it's, therefore, necessary to identify internal variables that reflect the damage level in the material. The most advanced method for a non-destructive quantitative evaluation of damage progression is the Acoustic Emission (AE) technique. Physically, AE is a phenomenon caused by a structural alteration in a solid material in which transient elastic-waves, due to a rapid release of strain energy, are generated. AEs are also known as stress-wave emissions.

In the present work a version of the Discrete Element Method built by bars (LDEM) are employed. This approach pertains to the alternative set of computational methods called by Munjiza [3], "Computational Mechanics of Discontinua" introduced during the 1960s, which is characterized by the lack of differential or integral equations to describe the model to study the space domain. In the mentioned approach, the behavior of the solid is function of the individual elements, e.g., particles or bars.

Here three tests are simulated to illustrated different characteristic of this approach applied in the

simulation of AE tests in quasi-brittle materials. The results obtained in terms of the global stress-strain response, the energy balance and the final configurations are presented. Also, the acceleration is registered in points of the specimen's surface and interpreted as data provided by a real device AE.

2. ACOUSTIC EMISSION

Acoustic Emission (AE) techniques constitute a very powerful approach to monitor the process of damage in structural systems, and have therefore found numerous applications in Civil, Mechanical, Aeronautical and other engineering branches. Acoustic Emission (AE) refers to the process in which micro fractures in the interior of a structural system cause elastic waves that propagate through the system and are therefore susceptible to detection by means of sensors, usually located on free surfaces [4]. AE events typically produce waves with frequencies in the range between 1 kHz and 1 MHz and amplitudes that depend on the amount of energy liberated and on the distance from the fracture to the sensor.

Traditionally, in AE testing, a number of parameters are recorded from the signals such as arrival time, velocity, amplitude, duration and frequency. From these parameters, damage conditions and localization of AE sources in the specimens are determined. It is possible to use the AE to compute a global parameter using the AE events, examples of this approaches are presented in [5–7]. The simulation of AE events and computation of global parameter such as *b*-value and RA and AF parameters using the LDEM was explored in Iturrioz et al. [8, 9] and Birck et al. [10]. In the present work, AE results are directly confronted with other results obtained in the simulation.

3. DISCRETE ELEMENT METHOD

3.1 Basic Formulation

The Lattice Discrete Element Method (LDEM) used in this work represents the continuum by means of a periodic spatial arrangement of bars with the masses lumped at their ends. The discretization strategy, shown in Figure 1, follows Nayfeh and Hefzy [11]. This method uses a basic cubic module constructed with twenty bars and nine nodes. Every node has three degrees of freedom, which are the three components of the displacement vector in the global reference system.

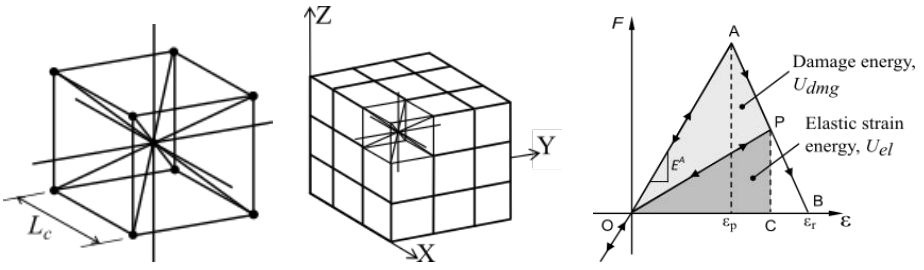

(a) (b) (c)

Figure 1. LDEM Discretization strategy: (a) basic cubic module, (b) prism formed using several cubic modules and, (c)Bilinear constitutive model with material damage.

In the case of an isotropic elastic material, the equivalent axial stiffness per unit length of the longitudinal elements (located along module edges and connecting the nodes in the center of the modules) is shown in Equation (1).

$$E_l^A = A_l E = \Phi E L_c^2, \tag{1}$$

where A_l is the cross section area of the element and E is the Young's modulus of the discretized

solid. The function $\Phi = (9+8\delta)/(18+24\delta)$, where $\delta = 9\nu/(4-8\nu)$, accounts for the effect of the Poisson's ratio ν [11, 12]. Similarly, the stiffness for the diagonal elements with area A_d is,

$$E_d^A = A_d E = \frac{2}{\sqrt{3}}\delta\Phi E L_c^2. \tag{2}$$

The coefficient $2/\sqrt{3}$ in Equation (2) accounts for the difference in length between the longitudinal and the diagonal elements, i.e., $L_d = 2/\sqrt{3}\, L_c$.

It is important to point out that for $\nu = 0.25$, the correspondence between the equivalent discrete solid and the isotropic continuum is complete. On the other hand, discrepancies appear in the shear terms for values of $\nu \neq 0.25$. These discrepancies are small and can be neglected in the range $0.20 \leq \nu \leq 0.30$. For values outside this interval, a different array of elements for the basic module should be used. Notice that this lattice model can not exactly represent a local isotropic continuum media. It can also be argued that no perfect locally isotropic continuum exists in practical engineering applications. Isotropy in solids is a bulk property that reflects the random distribution of the constituent.

Newton's second law is enforced at every node to obtain the system of equations

$$\mathbf{M}\ddot{\mathbf{x}}(t) + \mathbf{C}\dot{\mathbf{x}}(t) + \mathbf{F}(t) - \mathbf{P}(t) = \mathbf{0}, \tag{3}$$

where vectors $\ddot{\mathbf{x}}(t)$ and $\dot{\mathbf{x}}(t)$ contain respectively the nodal accelerations and velocities; $\mathbf{M}$ and $\mathbf{C}$ are the mass and damping matrices, respectively, the vectors $\mathbf{F}(t)$ and $\mathbf{P}(t)$ contain respectively the internal and external nodal forces. Since $\mathbf{M}$ and $\mathbf{C}$ are diagonal, the equations are not coupled, and they can be easily integrated in the time domain using an explicit finite difference scheme.

It is worth noting that since nodal coordinates are updated at every time step, large displacements are accounted without extra computation because the model maintains the objectivity with finite displacement. At the same time, the LDEM has a natural ability to model cracks. They can be introduced into the models as pre-existent features or as the irreversible effect of crack nucleation and propagation. Crack nucleation and propagation require non-linear constitutive models for material damage in order to allow the elements to break when they reach a critical condition. The details about the formulation and implementation of these non-linear constitutive models are given in the next section.

3.2 Non-linear constitutive model to account for anisotropic damage

Rocha et al. [13], and more recently Kosteski et al. [14], introduced non-linear constitutive models to account the reduction in the element load carrying capacity due to the irreversible effects of crack nucleation and propagation. The bilinear model for quasi-brittle materials proposed by Rocha et al. [13] is used in this work and it will be briefly presented next. The readers are referred to the above references for further details.

The area under the force versus strain curve (the area of the triangle OAB in Figure 1c) is the energy density required to fracture the area of influence of the element. Thus, for a given point P on the force vs. strain curve, the area of the triangle OPC represents the reversible elastic energy density stored in the element, while the area of the triangle OAP is the dissipated fracture energy density. Once the dissipated energy density equals the fracture energy, the element fails and loses its load carrying capacity. On the other hand, in the case of compressive loads the material behaves as linear elastic. Thus, the failure under compression load is induced by indirect traction. This assumption is reasonable for quasi-brittle materials for which the ultimate strength in compression is usually from five to ten times larger than that in tensile (see 15).

The parameters for the constitutive model in Figure 1(c) are (see 13):

- *Force*, F: this is the element axial force as a function of the longitudinal strain ε.
- *Element stiffness*, E_i^A: depending whether longitudinal or diagonal element is considered, E_d^A or E_l^A is adopted, see Equations (1) and (2).
- *Length*, L_c: length of the LDEM basic cubic module (see Figure 1a).
- *Specific fracture energy*, G_f: the fracture energy per unit area, which is coincident with the material fracture energy, G_c.
- *Equivalent fracture area*, A_i^f: where i could be l or d depending whether a longitudinal or a diagonal element, respectively. This parameter enforces the condition that the energy dissipated by the fracture of the continuum is equivalent to that of its discrete representation. The energy dissipated by the fracture of a material sample of size $L_c \times L_c \times L_c$ due to a crack parallel to one of its faces is,

$$\Gamma = G_f \Lambda = G_f L_c^2. \tag{4}$$

The energy dissipated by the fracture of a LDEM module is,

$$\Gamma_{LDEM} = G_f c_A \left[(4)(0.25) + 1 + 4\left(\frac{2}{\sqrt{3}}\delta\right)\right] L_c^2, \tag{5}$$

where the first term accounts for the four edge normal elements, the second term for the internal longitudinal element, and the third term for the four diagonal elements. The factor $\frac{2}{\sqrt{3}}\delta$ in the third term is the stiffness ratio between the diagonal and the longitudinal bar, which is the quotient between Expressions (1) and (2). The coefficient c_A is the scaling parameter to establish the equivalence between Γ and Γ_{LDEM}, given by Equations (4) and (5), respectively. In the case $\nu = 0.25$ is adopted, it results:

$$G_f L_c^2 \cong G_f \left(\frac{22}{3} c_A\right) L_c^2, \tag{6}$$

from which the value $c_A \cong 3/22$ is obtained.

Finally, the equivalent fracture areas of longitudinal and diagonal elements are:

$$A_d^f = \frac{4}{22} L_c^2, \tag{7}$$

and,

$$A_l^f = \frac{3}{22} L_c^2, \tag{8}$$

for the diagonal and longitudinal elements, respectively.

- *Critical failure strain*, ε_p: The so-called critical strain ε_p, as illustrated in Figure 1(c), is the maximum strain before the damage initiation. ε_p is a micro-parameter, i.e., a parameter that governs the constitutive law at the bar level. Young's modulus E, the stress intensity factor K_c and the critical stress ε_p are related by the classical fracture mechanic expression [16] given below:

$$K_c = \sigma_p Y \sqrt{\pi d} = E \varepsilon_p Y \sqrt{\pi d}, \tag{9}$$

in which Y is a parameter that accounts for the influence of the boundary conditions and the orientation of the critical fissure of size d. If the behavior is assumed up to the initiation of rupture is linear, then $\sigma_p = E\varepsilon_p$ and, recalling the equivalence between K_c and the specific facture energy G_f , we obtain the expression:

$$\sqrt{G_f E} = E \varepsilon_p Y \sqrt{\pi d}. \tag{10}$$

In order to simplify Equation (10), an equivalent length d_{eq} is defined as follows:

$$d_{eq} = d\pi Y^2. \tag{11}$$

Substituting Equation (10) in (11), then:

$$d_{eq} = \frac{G_f}{\varepsilon_p^2 E}. \tag{12}$$

Equation (12) indicates that d_{eq} may be regarded as a material property, since it does not depend on the discretization level, representing in fact a characteristic length of the material (similar as the width of the plasticity region in the head of the fissure in the Dugdale model). About this topic, see a classical Fracture Mechanics book as Kanninen and Popelar [16]. The link between the critical size concepts introduced by Taylor [17] is evident. Isolating the critical strain in the Expression (12), one can obtained:

$$\varepsilon_p = \sqrt{\frac{G_f}{d_{eq} E}}. \tag{13}$$

- *Limit strain*, ε_r: it is the strain value for which the elements lose their load carrying capacity (point B in Figure 1c). The limit strain is expressed in terms of the critical strain:

$$\varepsilon_r = K_r \varepsilon_p, \tag{14}$$

where,

$$K_r = \left(\frac{G_f}{E\varepsilon_p^2}\right)\left(\frac{A_i^f}{A_i}\right)\left(\frac{2}{L_i}\right) = \left(d_{eq}\right)\left(\frac{A_i^f}{A_i}\right)\left(\frac{2}{L_i}\right). \tag{15}$$

Notice that in order to guarantee the stability of the method, the condition $K_r \geq 1$ must be satisfied. This condition is enforced by using the restriction $L_i \leq L_{cr}$ on the element length with:

$$L_{cr} = 2\left(\frac{G_f}{E\varepsilon_p^2}\right)\left(\frac{A_i^f}{A_i}\right) = 2\left(d_{eq}\right)\left(\frac{A_i^f}{A_i}\right), \tag{16}$$

for both, the longitudinal, $i = l$, and the diagonal elements, $i = d$. The values for the element cross sectional areas, A_i, are in Expressions (1) and (2), while the equivalent fracture areas, A_i^f, are those in Equations (7) and (8).

Also notice that, in contrast to the usual practice in finite elements, the constitutive relationship in the LDEM is not only a function of the material properties. The element constitutive relationship presented in Figure 1(c) is defined in terms of parameters depending on material properties (ε_p, E, d_{eq} and G_f), model discretization (L_c, A_i^f) or both of them (E_d^A and ε_r). For this reason, when the discretization level is changed, the uniaxial constitutive law used in each bar must be modified.

A second interesting feature of the method is that although it uses a scalar damage law to describe the uniaxial behaviour of the elements, the global model accounts for anisotropic damage, since the elements are orientated in different spatial directions.

The randomness of the model is introduced considering G_f as a random field with a Weibull density function characterized by a mean $\mu(G_f)$ and a coefficient of variation $CV(G_f)$. It is also necessary to consider the spatial correlation function of this random parameter. In the present version of LDEM, the correlation function is considered constant, meaning that in the interval of the correlation length $L_{corr} = 2L_c$.

The introduction of small perturbations of the cubic arrangement, generated by small initial displacements of nodal points, should also result in small changes in the stiffness of the elements. Hence, it is herein assumed that the stiffness coefficients of the LDEM model remain unaltered by small perturbations of the mesh. Moreover, the linear response of the model should remain unaltered within the range of interest. Basically, it is assumed that the nodes in the perturbed model are displaced from their position in a perfect cubic arrangement, defined by nodal coordinates (x_n , y_n , z_n), as indicated in Equation (17).

$$(x_n + r_x(L_c), y_n + r_y(L_c), z_n + r_z(L_c)), \tag{17}$$

where r_x, r_y and r_z are random numbers with a normal distribution, zero mean and coefficient of variation CVp. L_c denotes the length of the longitudinal elements in the cubic cell. The CVp value that best fits the experimental evidence was determined by numerical experimentation [9, 18], ie, $CVp = 2.5\%$. The introduction of this type of perturbation in the mesh is fundamental to improve the model performance in modelled specimens submitted to compression stress. In Iturrioz et al. [8, 9] more details about the mesh perturbation are presented.

4. APPLICATIONS

4.1 Concrete notched beam

In the present case, a plain concrete beam, with pre-notched and depth equal to half the overall height, was simulated to a three-point bending (TPB). In Cartinteri et al. [19] the experimental results of this structure are presented. Standards results as force and vertical deflection were computed and AE test was performed. The scheme, main geometrical parameters, and the general aspect of the discretization used are reported in Figure 2. The material properties are: Young's modulus 12.5 GPa; Poisson's ratio 0.25; density 2800 kg/m^3, and specific fracture energy (Gf) 70 N/m. The beam was discretized with 168x20x20 basic cubic with length (L_c) equal 5 mm.

In Figure 3(a), the experimental and simulation result in terms of the global beam load vs. midspan displacement are presented. In Figure 3(b), the energy balance obtained in the simulation is showed.

Notice in the Figure 3(a), that the experimental and numerical results are quite good up to 0.3 mm in the midspan deflection, the softening branch in the numerical curve is more pronounced that the experimental one. The reason for this different behaviour is due to the experimental test was tested up

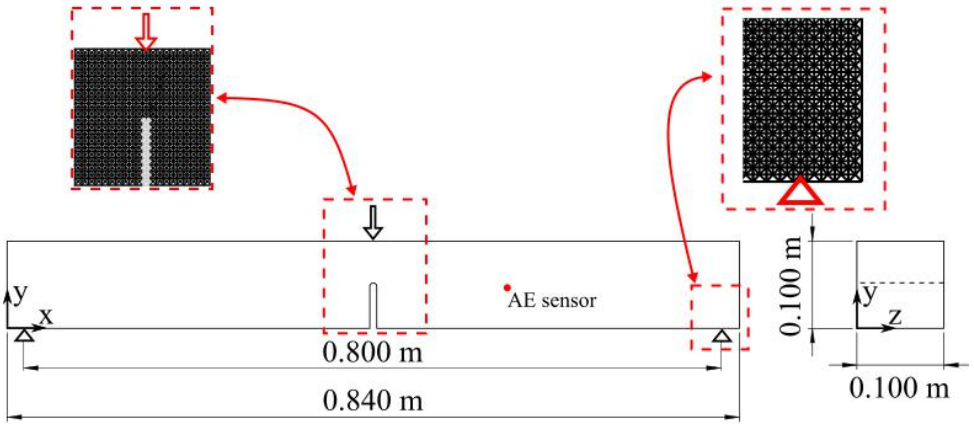

Figure 2. Scheme and geometrical parameters of the notched concrete beam and LDEM details.

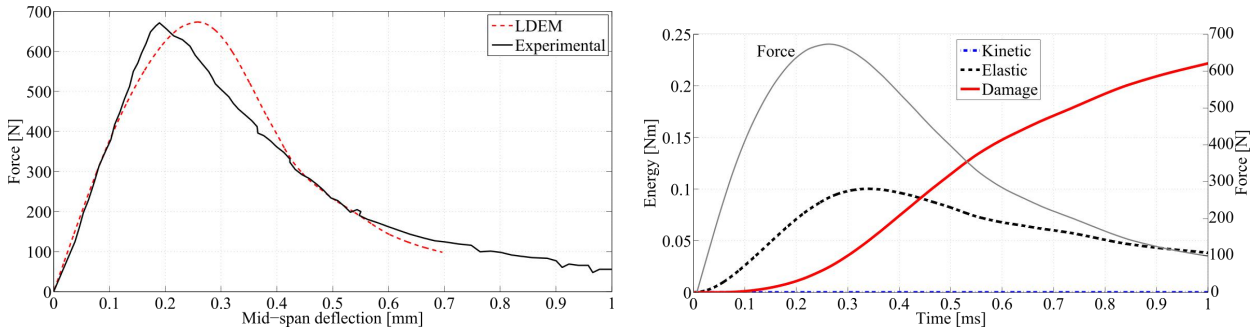

(a) (b)

Figure 3. (a) Load vs. midspan deflection for numerical and experimental TPB test. (b) Numerical energy balance.

to final failure by controlling the crack mouth opening displacement with constant opening velocity and in the model this condition was not applied. In the Figure 3(b), the energy balance during all the simulation is presented. Observe here that, the damage process occurs during all the simulation without avalanche or abrupt events, that is, the beam breaks smoothly.

In the Figure 4, Acoustic Emission signal is presented. In this figure, it is possible perceive the sequence of events simulated. The sensor was positioned in the red point indicated in Figure 2. This acoustic events consist on to save the acceleration in normal direction respect the specimen surface where the virtual sensor is positioned.

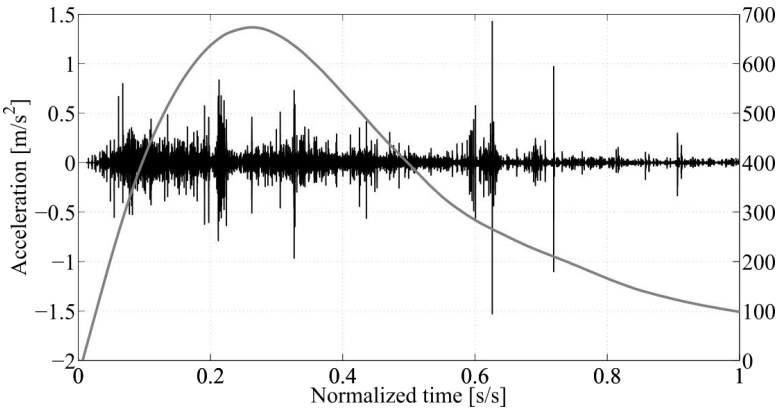

Figure 4. Acoustic Emission signal obtained with LDEM.

The magnitude of the critical strain vs. the normalized time is presented in Figure 5. Notice that

the value of critical strain ε_p (defined in the Figure 1c) is a random variable. In this figure, a tendency cannot be seen, i.e., the weak bars didn't break first. This is because there is a stress concentration since the beginning of the process (there is a notch in the middle of the beam).

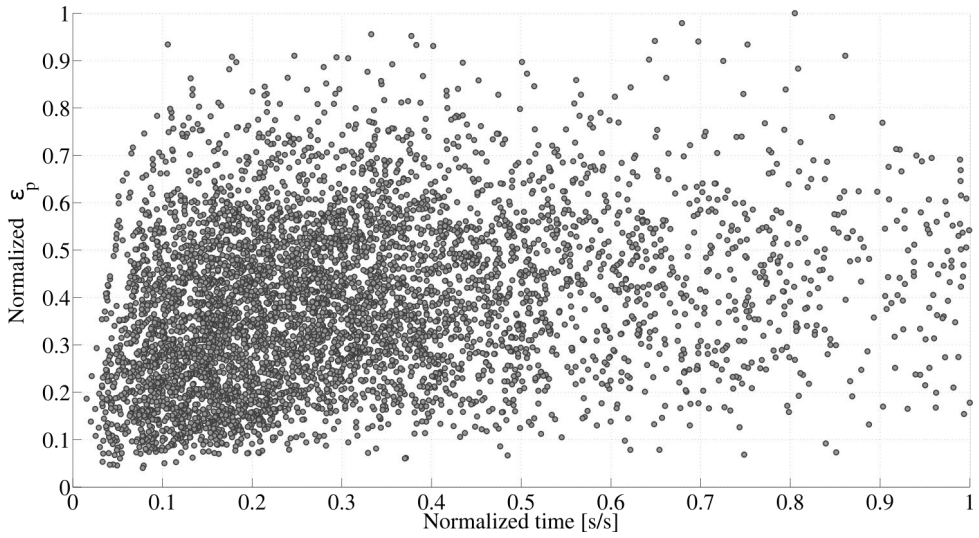

Figure 5. Numerical results in terms of critical strain vs. normalized time.

The location and when the bar critical strain (ε_p) is reached are shown in Figure 6. In this figure, the distribution of the damage during the damage process is available. Finally in the Figure 7, the configuration in 88.8% of the time and a detail obtained with LDEM are presented.

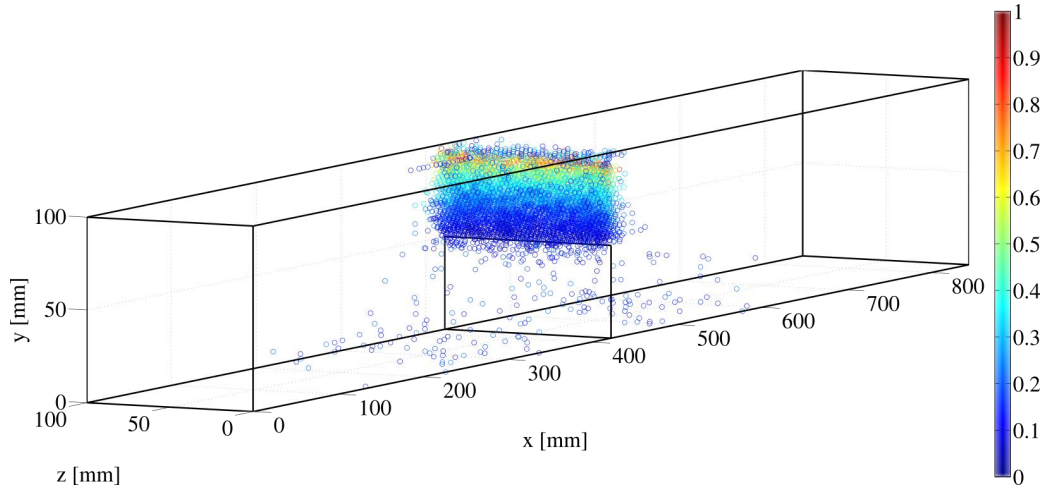

Figure 6. Results in terms of temporal and spatial distribution when the critical strain is reached. The color scale is the normalized time.

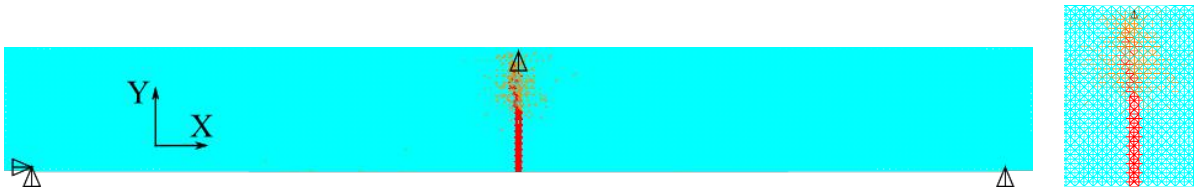

(a) (b)

Figure 7. Configuration in 88.8% of the time: (a) global view, and (b) detail.

4.2 Plate submitted to shear solicitation with different levels of compression

The fracture process of a square plate subjected to support displacements that induce an homogeneous pure shear excitation with linearly increasing amplitude is analysed by numerical simulation. Attention will be centred on the LDEM predictions of AE. Dimensions and material properties of the plate, indicated next, were chosen in order to allow a future experimental verification of the results. E=32 GPa, ρ =2400 kg/m^3, G_f= 70 N/m and tensile strength σ_t= 5 MPa. The sides of the plate are 50 cm long and its thickness 4 cm. In Figure 8,a plan of the plate, the boundary conditions and the spatial distribution of virtual AE sensors are presented. The AE sensor record the motion in the direction normal to the middle plane of the plate. The LDEM model consisted of $125 \times 125 \times 10$ cubic cells with 4mm length. The basic parameters are indicated in Table 1, and the parameters $\varepsilon_p = 3.34 \times 10^{-4}$ and K_r =3.3, which completely characterize the constitutive law shown in Figure 1(c).

Table 1. Parameters of LDEM model of the plate.

L	4mm	d_{eq}	20mm
$\mu(G_f)$	70 N/m	ν	0.25
$\mu(E)$	32 GPa	ρ	2400 kg/m^3
$CV(G_f)$	1.0	$CV(E)$	1.0

Also in the present case, the results in terms of the magnitude of the critical strain that is reach during the damage process is presented in Figure 9(a). In the Figure 9(b) the spatial and time distribution of bars that reach the critical strain is presented. In both figures, the case presented is when only shear stress in the boundaries is applied.

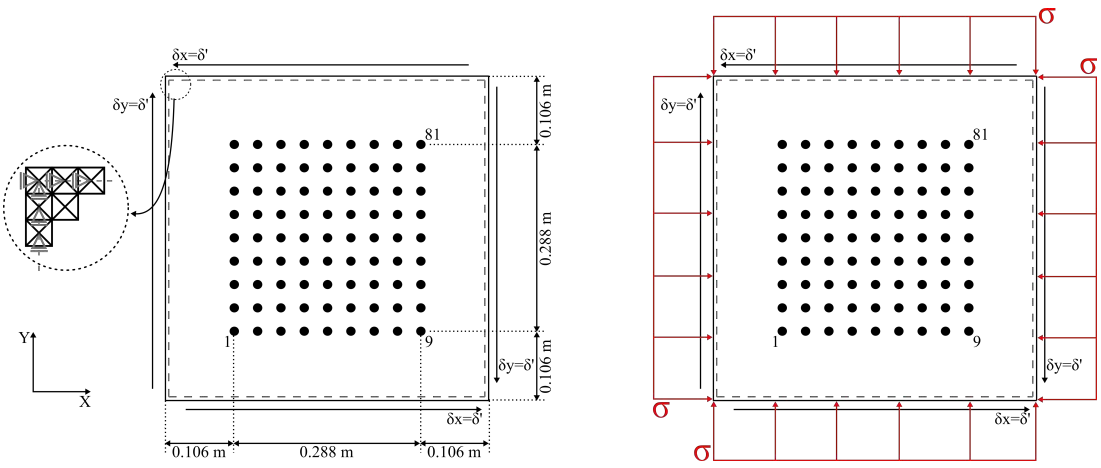

Figure 8. Shear test (on the left) and shear and compression test (on the right).

The rupture in pure shear test increase with little spasmodic avalanches that appear in the Figure 9(a) as vertical line of circles, up to arrive to the final rupture. Finally in this application, the AE signal for the three cases simulated, the first a shear stress without pre-compression, and the second and third with different levels of pre-compression are presented in Figure 10. Notice that the levels of pre-compression produce a change in the general aspect of the AE record that is when increase the pre-compression the specimen turn more ductile and the final rupture happen after.

4.3 The cylinder submitted to diametral load

Difficulties presented by the direct tensile test of non-homogeneous materials were circumvented by the indirect tensile test proposed for concrete by Lobo Carneiro in 1943, which found applications

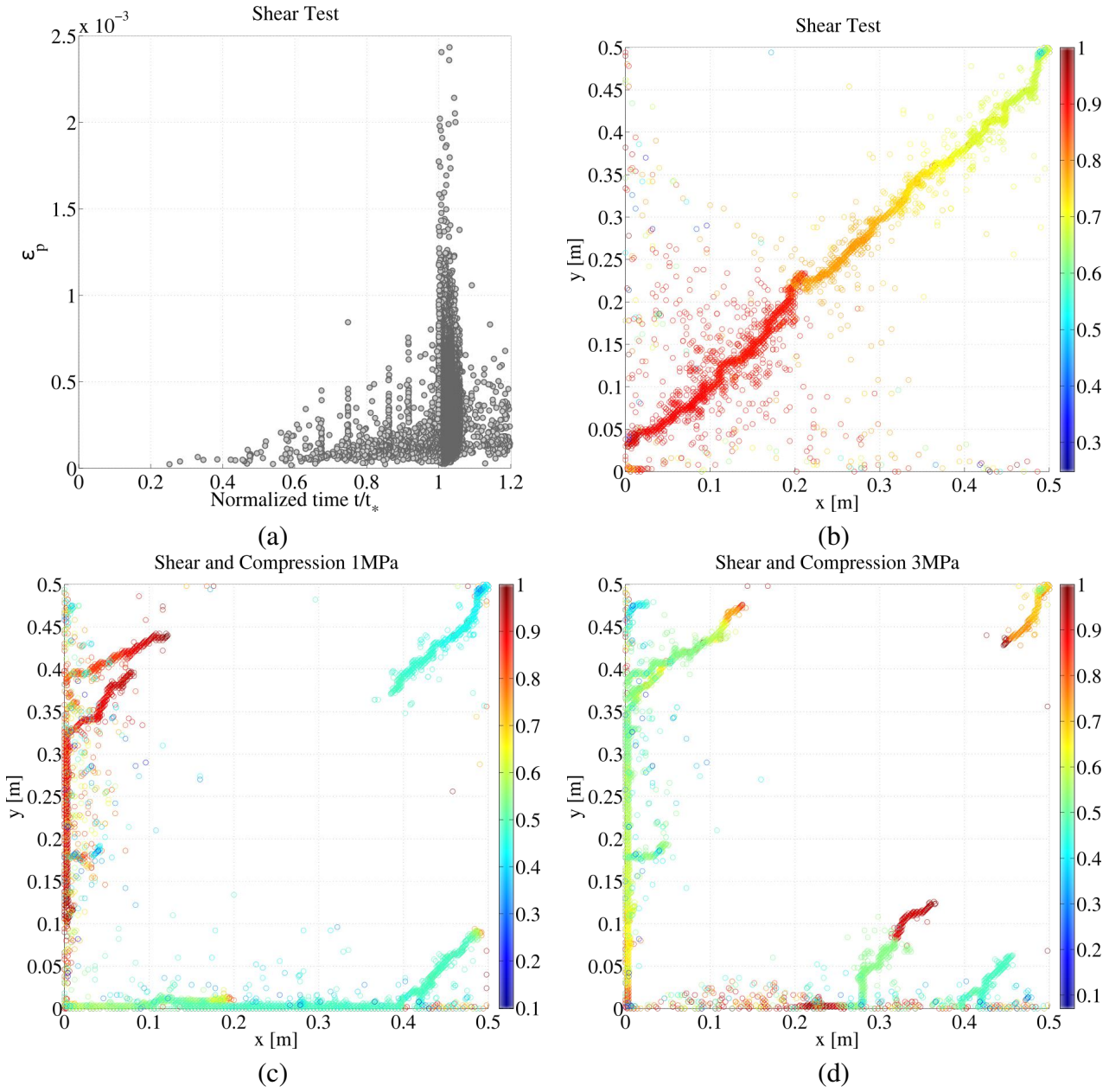

Figure 9. (a) Critical Strain vs. Normalized Time for the pure shear test. The spatial and temporal distribution of critical strain for (b) pure shear model, (c) shear with 1MPa of compression and,(d) shear with 3 MPa of compression.

in the technology of concrete, rocks, ceramics and other materials and it is today known worldwide as the Brazilian test. The relations between predictions of the Brazilian test and results of both the direct tensile test and the unconfined compression test have been subject of extensive studies based on experimental evidence in the last half century. On the other hand, developments in the numerical fracture analysis of non-homogeneous materials allowed detailed examinations of the rupture process in the test, considering also scale and rate effects. The Lattice Discrete Element Method with mesh imperfections was recently applied by Riera et al. [18] to predict the response of simulated concrete samples subjected to indirect tensile tests. The approach was later extended by Miguel et al. [20] to more precisely quantify the role of factors such as the width and stiffness of the strips inserted between the press platens and the sample cylinders. It was shown that the flexibility of the strip exerts a marginal influence on the result of the test, especially for relative width β (ratio between the width

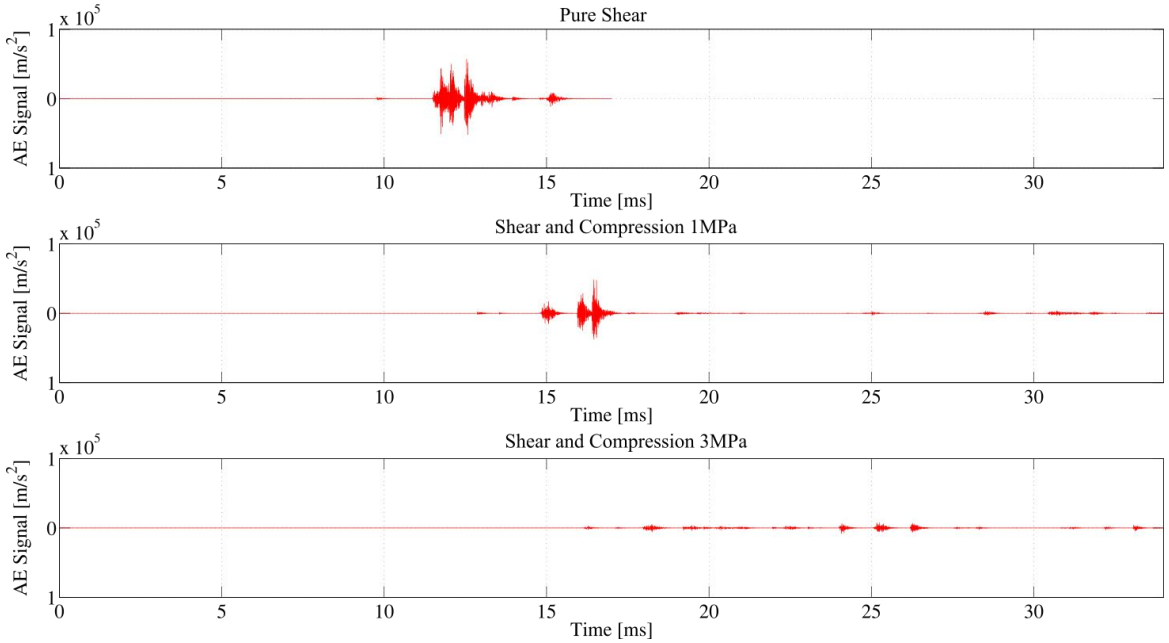

Figure 10. AE signal with the vertical axis in the same scale.

Table 2. Parameters adopted in LDEM model.

Total number of nodes	18086	Damping factor	0.500000E+03
Total number of elements	14085	Basic module length	3.75000E-03 m
Integration time step	0.500000E-06 s	Poisson's ratio	0.25
Total time of integration	0.200000E+00 s	Specific mass	2300 kg/m^3
Total mass	0.970312E+00 kg	Young's modulus	0.300000E+11 Pa
Longitudinal element stiffness	0.170814E+06	Critical value for L_c	0.721354E-01
Diagonal element stiffness	0.295859E+06	Proportionality mean strain	0.169706E-03
Specific fracture energy G_f	0.900000E+02	Coefficient of variation of G_f	0.6
Mean value for failure agent	0.300000E+01	K_r value for normal bars	0.192361E+02

of the strip and the sample diameter) around 0.25.

In the present application, the influence of the orientation of the LDEM mesh on the resulting indirect tensile strength on Brazilian test disks with $\beta = 0.225$ loaded width is evaluated.

As explained above, cylindrical disks with 150mm diameter and 18.75mm thickness were analysed by means of LDEM models with 40 basic modules in each the x and y directions, and 5 modules in the z direction. The modulus length was $L = 3.75$mm. The lateral loads were applied as prescribed displacements in the radial direction, within a loaded width corresponding to β= 0.225, as shown in Figure 11 in the radial orientation. It should be recalled at this point that prior to the introduction of the random distribution of material properties and of the perturbation of the LDEM cubic arrangement of nodal points, the coordinate axes x and y define symmetry planes.

It is used in the present case $c_p = 7.5\%$ as level of mesh perturbations. Moreover, in the simulated tests, plane strain conditions are assumed. To avoid or at least reduce the initiation of fractures in the regions of load application, the critical strains of elements within the green regions of Figure 11 were increased by a factor of 2, while nodal coordinated remained with their unperturbed values. Other parameters adopted in the numerical models are given in Table 2.

Three typical final configurations obtained with LDEM are shown in Figure 12, and the patterns presented in this figure can be compared with experimental results, presented in Figure 13, showing similar ones.

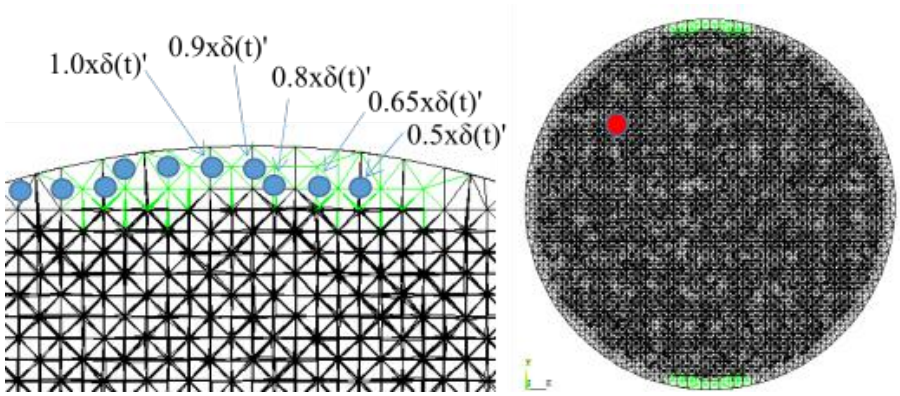

Figure 11. Disk loaded along vertical (nominal) symmetry axis (0°). Nodes with specified vertical displacements are indicated at left. Loaded region corresponds to β= 0.225. The red circle indicate where the AE sensor was positioned.

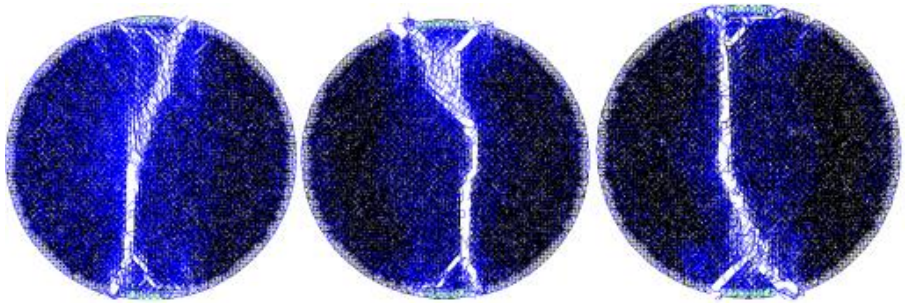

Figure 12. Results in terms of LDEM final configurations, three simulations using CV_p=7.5%.

Figure 13. Experimental results obtained in UNIPAMPA (Alegrete Brazil, Kosteski). In body tests of 150 mm of Diameter.

In the Figure 14, it is shown how the damage increases during the simulation, the damage bars are in blue, the broken bars in red and, the undamaged bars are not presented. Notice that up to around $t/t_r = 0.4$ the damage evolved in the vertical direction close the central region (marked with a box), then the damage begin to expand also in the horizontal region when this damage region adopt a bulb shape. After the formation of the bulb shape, different focus of localization appears and finally the localization happens and the specimen breaks abruptly.

Acoustic Emission signal emission measured in the red point, indicated in the Figure 11, is presented in the Figure 15(a). The spatial distribution of the bars that broke over time is shown in the Figure 15(b). In this figure, the vertical axis is the normalized time (the same information is indicated with the color rule) and in the horizontal axis indicate the diameter dimension in vertical direction [m].

As can be seen in Figure 15(a), defined AE events didn't appear until $t/t_r = 0.4$, this part is characterized by Poisson process; after $t/t_r = 0.4$ isolated AE events happens, indicating that the process of localizations of the damage begun.

In the Figure 15(b), the results in terms of the time and the bars position that reach the critical strain,

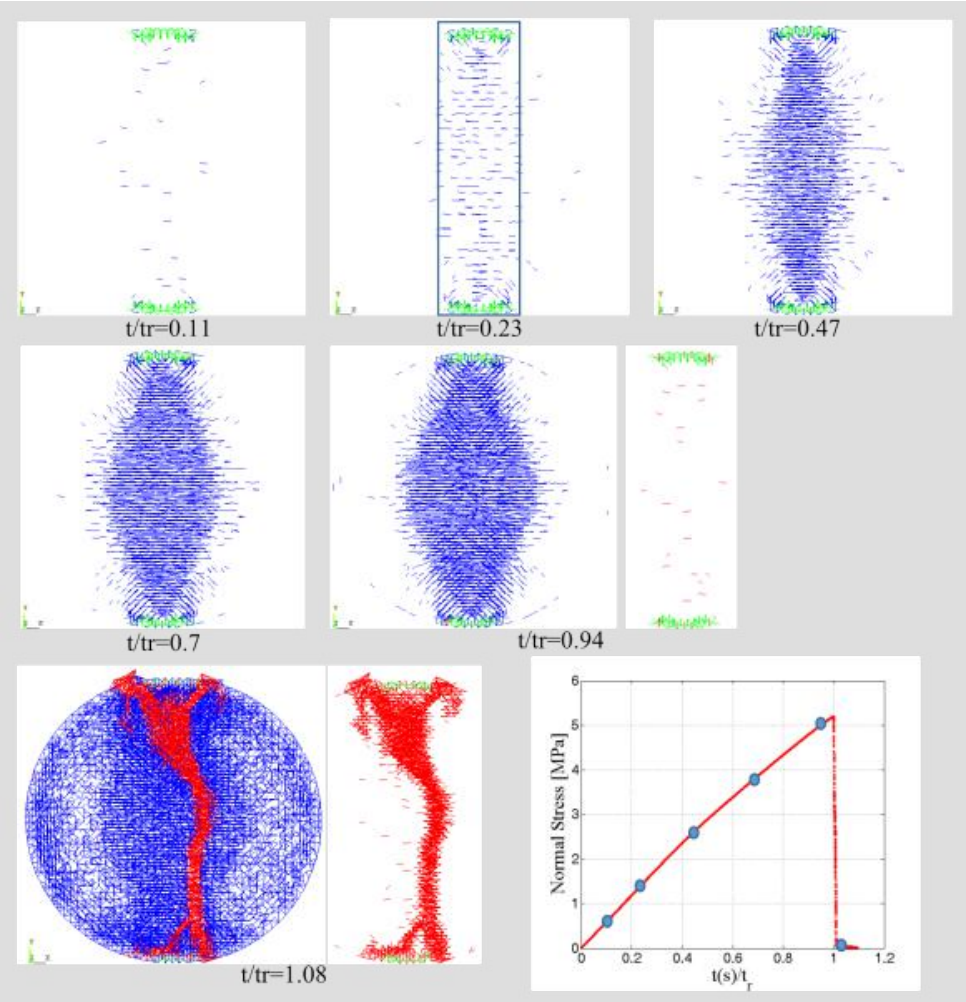

Figure 14. Sequence of configurations that shown how the damage grow during the simulation.

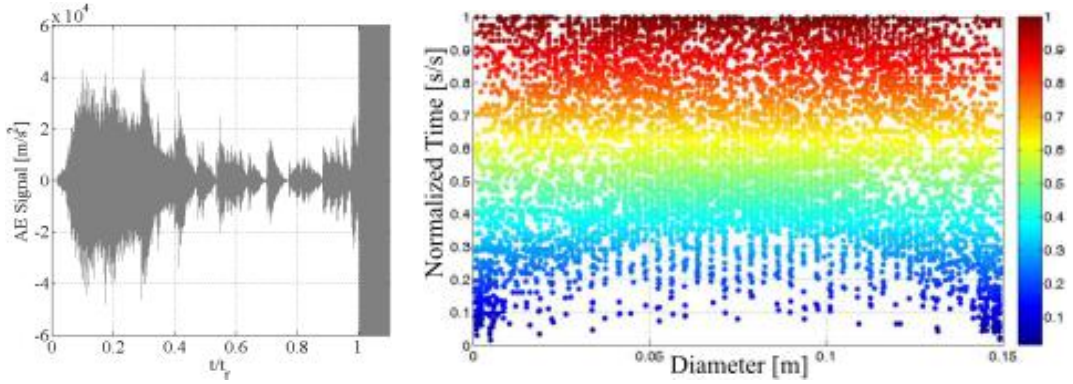

(a) (b)

Figure 15. Results in terms of: (a) Acoustic Emission, and (b) the temporal and spatial distribution of the elements that reached the critical strain.

only the vertical coordinate, are presented. Notice that in the beginning some few bars break close the boundaries and then the distribution of the damage happen on all the central line of the specimen. After $t/t_r = 0.4$ a more density of point clearly appear in the plot due to this point correspond not only of damage bar in a thin volume around the transversal section but also in a bulb volume with tendency to grow its central part.

The magnitude of the critical strain reach for the bar in the time are presented in the Figure 16. As

can be seen, after a disorganized begin (up to $t/t_r = 0.05$) the values of strain appear over an inclined line tendency, up to arrive the value of $t/tr = 0.4$. After this time the damage process changed. The same information could be appreciated in the Figure 15 in terms of the Acoustic Emission distribution, or spatial distribution of bars that arrive to the critical strain.

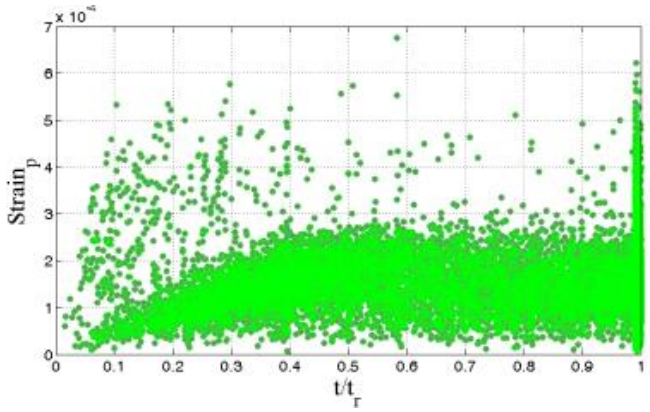

Figure 16. The magnitude of the critical strain reaches for each bar vs the normalized time during the simulation.

4.4 Results comparison

It is possible to compare some aspects about how the different specimens coming to the failure:

i) In the first application, a notch beam produce a high gradient of stress close the fissure ahead, in this case the random spatial distribution of the critical strain have a marginal effect, this fact is clearly observed in Figure 5, where no tendency appear in the sequence of the bars rupture.

ii) In the second application, the damage is more uniformly distributed over the plate submitted to shear solicitation during the process. This is clearly indicated in the Figure 9(a), where weaker bars broken before, showing a linear tendency in the beginning of the damage process, then sets of bars had broken in the same time characterizing an spasmodic behaviour and indicating an avalanche behaviours.

iii) In the third application, a more stable diffuse growing of damage happen up to $t/t_r = 0.4$, this appear clearly in the Figures 15 and 16, in the last mentioned figure a clearly linear declivity indicates a tendency of weaker bars break first. In the same figure also appears a few more strength bars broken in the beginning of the process. These last bars are situated close the support regions where some stress concentration happen.

5. CONCLUSIONS

In the present work, the possibility of the Lattice Discrete Element Method to simulate the fracture process in Quasi-Brittle material is explored. Three different applications are presented and it was possible conclude that:

- The Acoustic Emission simulation and the possibility to confront the simulation with experimental results could be a powerful tool to understand the damage process in this kind of materials.

- It was possible describe in different ways how the specimen coming to the failure. This information complements the Acoustic Emission data, and let a better interpretation of these results.

6. ACKNOWLEDGEMENTS

The authors wish to thank the Brazilian agencies CNPq and Capes for funding this research.

REFERENCES

[1] Lemaitre, J. and Chaboche, J.-L. (1990). Mechanics of solid materials. Cambridge: University Press.

[2] Krajcinovic, D. (1996). Damage mechanics, volume 41. Elsevier, Amsterdam.

[3] Munjiza, A. (2009). "Special issue on the discrete element method: aspects of recent developments in computational mechanics of discontinua." Engineering Computations, 26(6).

[4] Grosse, C. U. and Ohtsu, M. (2008). Acoustic Emission Testing. Springer Berlin Heidelberg. ISBN 9783540699729.

[5] Colombo, I. S., Main, I., and Forde, M. (2003). "Assessing damage of reinforced concrete beam using "b-value" analysis of acoustic emission signals." Journal of materials in civil engineering, 15(3):280–286.

[6] Shiotani, T., Fujii, K., Aoki, T., and Amou, K. (1994). "Evaluation of progressive failure using AE sources and improved b-value on slope model tests." Progress in Acoustic Emission, 7(7):529–534.

[7] Carpinteri, A., Lacidogna, G., and Niccolini, G. (2009). "Fractal analysis of damage detected in concrete structural elements under loading." Chaos, Solitons & Fractals, 42(4):2047–2056.

[8] Iturrioz, I., Lacidogna, G., and Carpinteri, A. (2013). "Experimental analysis and truss-like discrete element model simulation of concrete specimens under uniaxial compression." Engineering Fracture Mechanics, 110:81–98.

[9] Iturrioz, I., Riera, J., and Miguel, L. (2014). "Introduction of imperfections in the cubic mesh of the truss-like discrete element method." Fatigue & Fracture of Engineering Materials & Structures, 37(5):539–552.

[10] Birck, G., Iturrioz, I., Lacidogna, G., and Carpinteri, A. (2016). "Damage process in heterogeneous materials analyzed by a lattice model simulation." Engineering Failure Analysis, 70:157 – 176. ISSN 1350-6307. doi:http://dx.doi.org/10.1016/j.engfailanal.2016.08.004.

[11] Nayfeh, A. H. and Hefzy, M. S. (1978). "Continuum modeling of three-dimensional truss-like space structures." AIAA Journal, 16(8):779–787.

[12] Dalguer, L., Irikura, K., Riera, J., and Chiu, H. (2001). "The importance of the dynamic source effects on strong ground motion during the 1999 Chi-Chi, Taiwan, earthquake: Brief interpretation of the damage distribution on buildings." Bulletin of the Seismological Society of America, 91(5):1112–1127.

[13] Rocha, M. M., Riera, J. D., and Krutzik, N. J. (1991). "Extension of a model that aptly describes fracture of plain concrete to the impact analysis of reinforced concrete." In International Conference on Structural Mechanics Reactor Technology (SMIRT 11).

[14] Kosteski, L., Iturrioz, I., Batista, R. G., and Cisilino, A. P. (2011). "The truss-like discrete element method in fracture and damage mechanics." Engineering Computations, 28(6):765–787.

[15] Kupfer, H. B. and Gerstle, K. H. (1973). "Behavior of concrete under biaxial stresses." Journal of the Engineering Mechanics Division, 99(4):853–866.

[16] Kanninen, M. and Popelar, C. (1985). Advanced Fracture Mechanics. Oxford engineering science series. Oxford University Press. ISBN 9780195035322.

[17] Taylor, D. (2007). The theory of critical distances: a new perspective in fracture mechanics. Elsevier. ISBN 10: 0-08-044478-4.

[18] Riera, J. D., Miguel, L. F. F., and Iturrioz, I. (2014). "Study of imperfections in the cubic mesh of the truss-like discrete element method." International Journal of Damage Mechanics, 23(6):819–838.

[19] Carpinteri, A., Lacidogna, G., Corrado, M., and Battista, E. D. (2016). "Cracking and crackling in concrete-like materials: A dynamic energy balance." Engineering Fracture Mechanics. ISSN 0013-7944. doi:http://dx.doi.org/10.1016/j.engfracmech.2016.01.013.

[20] Miguel, L. F., Riera, J. D., Iturrioz, I., and Aráoz, G. F. (2016). "Influence of the Width of the Loading Strip in the Brazilian Tensile Test of Concrete and Other Brittle Materials." Journal of Materials in Civil Engineering, 28(11). doi:10.1061/(ASCE)MT.1943-5533.0001628.

RESPONSIBILITY NOTICE

The authors are the only responsible for the printed material included in this paper.